

Mitochondrial DNA stress primes the antiviral innate immune response

A. Phillip West¹, William Khoury-Hanold², Matthew Staron², Michal C. Tal²†, Cristiana M. Pineda¹, Sabine M. Lang¹, Megan Bestwick¹†, Brett A. Duguay³, Nuno Raimundo¹†, Donna A. MacDuff⁴, Susan M. Kaech^{2,5}, James R. Smiley³, Robert E. Means¹, Akiko Iwasaki^{2,5} & Gerald S. Shadel^{1,6}

Mitochondrial DNA (mtDNA) is normally present at thousands of copies per cell and is packaged into several hundred higher-order structures termed nucleoids¹. The abundant mtDNA-binding protein TFAM (transcription factor A, mitochondrial) regulates nucleoid architecture, abundance and segregation². Complete mtDNA depletion profoundly impairs oxidative phosphorylation, triggering calcium-dependent stress signalling and adaptive metabolic responses³. However, the cellular responses to mtDNA instability, a physiologically relevant stress observed in many human diseases and ageing, remain poorly defined⁴. Here we show that moderate mtDNA stress elicited by TFAM deficiency engages cytosolic antiviral signalling to enhance the expression of a subset of interferon-stimulated genes. Mechanistically, we find that aberrant mtDNA packaging promotes escape of mtDNA into the cytosol, where it engages the DNA sensor cGAS (also known as MB21D1) and promotes STING (also known as TMEM173)–IRF3-dependent signalling to elevate interferon-stimulated gene expression, potentiate type I interferon responses and confer broad viral resistance. Furthermore, we demonstrate that herpesviruses induce mtDNA stress, which enhances antiviral signalling and type I interferon responses during infection. Our results further demonstrate that mitochondria are central participants in innate immunity, identify mtDNA stress as a cell-intrinsic trigger of antiviral signalling and suggest that cellular monitoring of mtDNA homeostasis cooperates with canonical virus sensing mechanisms to fully engage antiviral innate immunity.

To explore the cellular responses to mtDNA stress in the absence of oxidative phosphorylation deficiency, we employed a TFAM heterozygous knockout (*Tfam*^{+/-}) mouse model. Cells and tissues from these animals exhibit modest or no significant differences in mtDNA-encoded transcripts and oxygen consumption rates, despite an approximately 50% depletion of mtDNA (Extended Data Fig. 1a–c)^{5,6}. In addition to mtDNA depletion, *Tfam*^{+/-} mouse embryonic fibroblasts (MEFs) have reduced oxidative mtDNA damage repair capacity and markedly altered mtDNA packaging, organization and distribution (Fig. 1a)⁶. Nucleoids in *Tfam*^{+/-} MEFs were less numerous and exhibited a larger size distribution (Fig. 1a and Extended Data Fig. 1d). Thus, *Tfam*^{+/-} cells provide a robust model to characterize cellular responses triggered by moderate mtDNA stress.

Gene expression profiling of *Tfam*^{+/-} MEFs revealed an unexpected enrichment of interferon-stimulated genes (ISGs) and antiviral signalling factors (Fig. 1b). Of the 45 most overexpressed genes, 39 were ISGs, including many with direct antiviral activity (*Ifi44*, *Ifit1*, *Ifit3*, *Oasl2*, *Rtp4*)^{7,8}. We also observed increased expression of cytoplasmic RNA and DNA sensors, such as *Ddx58* and *Ifih1* and p200 family proteins *Ifi203*, *Ifi204* and *Ifi205*, as well as transcription factors *Irf7*, *Stat1* and *Stat2*, ISGs that function to positively reinforce the antiviral response. Direct measurement of basal ISG mRNA and protein expression

in *Tfam*^{+/-} MEFs validated the microarray results (Fig. 1c, d). Finally, *Tfam*^{+/-} MEFs expressed three- to fourfold more *Ifnb* and *Ifna4* upon transfection with the IFI1 agonist poly(I:C) (Fig. 1e), consistent with enhanced type I interferon responses.

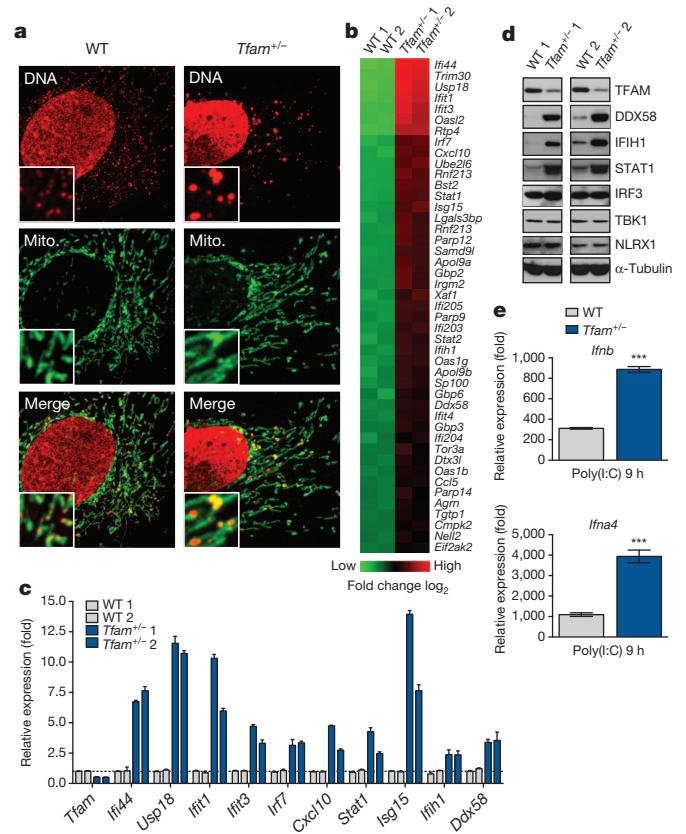


Figure 1 | *Tfam*^{+/-} cells exhibit mtDNA stress, elevated ISG expression and augmented type I interferon responses. **a**, Confocal microscopy images of MEFs stained with anti-DNA (DNA) and anti-HSP60 (Mito.) antibodies. **b**, Heat maps of microarray analyses. Genes in *Tfam*^{+/-} MEFs exhibiting statistically significant ($P < 0.05$), twofold or greater increases over wild type (WT) are shown. **c**, **d**, Quantitative real-time-PCR (qRT-PCR) (**c**) and western blots (**d**) of basal ISG expression in two littermate wild-type and *Tfam*^{+/-} MEF lines. **e**, qRT-PCR analysis of type I interferon expression in MEFs 9 h after cytosolic delivery of poly(I:C). Error bars indicate \pm s.e.m. of triplicate technical replicates and are representative of three independent experiments. *** $P < 0.001$.

¹Department of Pathology, Yale School of Medicine, New Haven, Connecticut 06520, USA. ²Department of Immunobiology, Yale School of Medicine, New Haven, Connecticut 06520, USA. ³Li Ka Shing Institute of Virology, Department of Medical Microbiology and Immunology, University of Alberta, Edmonton, Alberta T6G 2S2, Canada. ⁴Department of Pathology and Immunology, Washington University School of Medicine, St Louis, Missouri 63110, USA. ⁵Howard Hughes Medical Institute, Chevy Chase, Maryland 20815-6789, USA. ⁶Department of Genetics, Yale School of Medicine, New Haven, Connecticut 06520, USA. †Present addresses: Institute for Stem Cell Biology and Regenerative Medicine, Stanford University School of Medicine, Stanford, California 94305, USA (M.C.T.); Department of Chemistry, Linfield College, McMinnville, Oregon 97128, USA (M.B.); Institute for Cellular Biochemistry, Universitätsmedizin Göttingen, 37073 Göttingen, Germany (N.R.).

To ensure that the mtDNA stress and ISG expression phenotypes were not unique to *Tfam*^{+/-} MEFs, we employed inducible TFAM depletion models (TF^D). Analogous to *Tfam*^{+/-} cells, TF^D MEFs and bone-marrow-derived macrophages (BMDMs) displayed mtDNA stress phenotypes, augmented ISG expression, and heightened type I interferon responses to poly(I:C) (Extended Data Fig. 1d–i). Collectively, these data indicate that TFAM depletion induces mtDNA nucleoid stress that triggers antiviral ‘priming’, characterized by basally elevated ISG expression and potentiated type I interferon production.

Since mitochondrial stress can trigger the release of mtDNA into the cytosol to engage the NLRP3 inflammasome, we assayed for extra-mitochondrial mtDNA in TF^D cells^{9,10}. Analysis of pure cytosolic extracts revealed a three- to fourfold increase of specific mtDNA fragments from the D-loop regulatory region, indicating liberation of immunostimulatory mtDNA into the cytosol (Extended Data Fig. 2)¹¹. Confocal and electron microscopy of TF^D cells revealed significantly elongated, interconnected mitochondrial networks consistent with a hyperfused phenotype (Fig. 1a and Extended Data Figs 1e, g and 3a, b). Since mitochondrial fission facilitates proper nucleoid distribution and removal of damaged mtDNA, we examined whether mitochondrial hyperfusion in TF^D cells governed mtDNA stress-induced ISG expression^{12,13}. Knockdown of mitofusin 1 (*Mfn1*) induced fission and largely abrogated ISG expression in TF^D MEFs (Extended Data Fig. 3c–e). Moreover, depletion of the mtDNA quality-control enzyme endo/exonuclease (5′–3′), endonuclease G-like (*EXOG*) exacerbated ISG expression in *Tfam*^{+/-} MEFs (Extended Data Fig. 3f)¹⁴. Collectively, these data indicate that TFAM depletion promotes accumulation of aberrant mtDNA, which accesses the cytosol to engage innate immune signalling.

We next examined the involvement of the cytosolic DNA sensor cGAS in mtDNA stress signalling, as it mediates ISG expression in response

to exogenous and endogenous immunostimulatory DNA species^{15–17}. Knockdown of cGAS in *Tfam*^{+/-} MEFs or TFAM depletion in *cGas*^{-/-} MEFs largely abrogated ISG expression (Fig. 2a). Furthermore, ISG mRNAs in TF^D cells were reduced 70–90% in the absence of STING, indicating cGAS–STING signalling is the predominant driver of mtDNA stress-induced ISG expression (Fig. 2b). STING signals via the TBK1–IRF3/7 axis to trigger antiviral gene expression, and knockdown of either TBK1 or IRF3 robustly blocked ISG expression in *Tfam*^{+/-} MEFs (Fig. 2c, d)^{18,19}. Consistent with IRF3 activating ISG transcription, we observed enhanced nuclear accumulation of IRF3 in TF^D cells (Fig. 2e). Finally, using *cGas*^{-/-} MEFs reconstituted with hemagglutinin (HA)-tagged, murine cGAS, we observed prominent re-localization of cGAS from nuclear and/or cytoplasmic pools to the vicinity of aberrant mtDNA nucleoids in TF^D MEFs (Fig. 2f, g). Taken together, these results indicate that mtDNA stress facilitates cGAS-dependent sensing of cytoplasmic mtDNA, resulting in STING–TBK1–IRF3 signalling to trigger ISG expression.

To establish functional significance of mtDNA stress-induced antiviral priming, we challenged MEFs with herpes simplex virus 1 (HSV-1) or vesicular stomatitis virus (VSV) that express green fluorescent protein (GFP) for easy detection. In contrast to wild-type cells, which displayed robust viral GFP expression post-infection, *Tfam*^{+/-} MEFs were markedly resistant to HSV-1 and VSV (Fig. 3a). In addition, *Tfam*^{+/-} MEFs exhibited heightened type I interferon and ISG expression upon viral challenge, consistent with potentiated type I interferon responses in these cells (Extended Data Fig. 4a). Similar results were obtained upon challenge with the rodent gammaherpesvirus MHV-68 (Fig. 3b and Extended Data Fig. 4b). Furthermore, TF^D BMDMs displayed augmented antiviral gene expression and markedly lower HSV-1- and VSV-encoded mRNA and protein 6–24 h post-infection (Extended Data Fig. 4c–f).

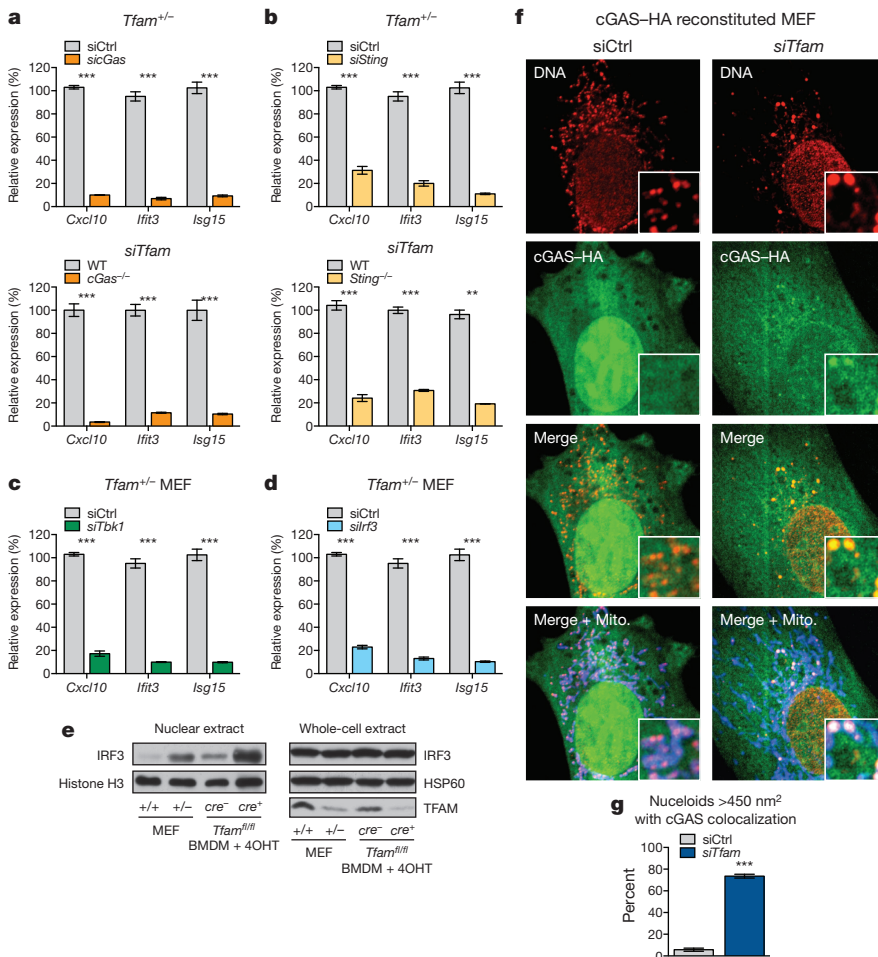


Figure 2 | mtDNA stress triggers ISG expression in a cGAS- and STING-dependent fashion.

a, b, ISG expression in *Tfam*^{+/-} MEFs transfected with the indicated short interfering RNAs (siRNAs; top panels), or wild-type (WT), *cGas*^{-/-} (a), and *Sting*^{-/-} (b) MEFs transfected with TFAM siRNAs (bottom panels). Ctrl, control. **c, d**, ISG expression in *Tfam*^{+/-} MEFs transfected with the indicated siRNAs for 96 h. **e**, Western blots of whole-cell and nuclear extracts of wild-type and *Tfam*^{+/-} MEFs or *Tfam*^{fl/fl} *ER-cre*^{+/-} (*cre*^{+/-}) BMDMs exposed to 4-hydroxytamoxifen (4OHT) for 96 h. **f, g**, *cGas*^{-/-} MEFs reconstituted with cGAS-HA were transfected with the indicated siRNAs for 96 h, then stained with anti-DNA (DNA), anti-HSP60 (Mito.) and anti-HA (cGAS-HA) antibodies and imaged. cGAS co-localization scoring was performed as described in the Methods. Error bars indicate \pm s.e.m. of triplicate technical (a–d) or biological (g) replicates and are representative of three independent experiments. **P* < 0.05; ***P* < 0.01; ****P* < 0.001.

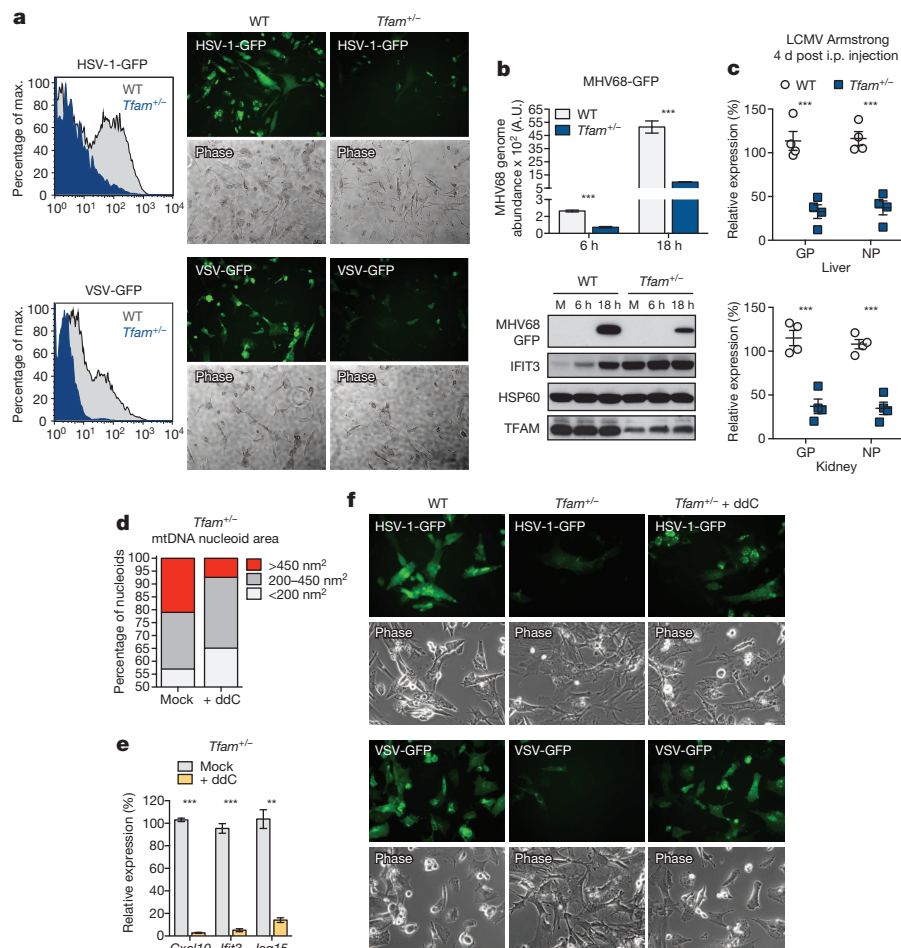


Figure 3 | mtDNA stress potentiates viral resistance. **a**, Viral GFP expression in MEFs infected with HSV-1-GFP or VSV-GFP at multiplicity of infection (MOI) 0.5 for 24 h. **b**, MHV68-GFP abundance and ISG expression in MEFs infected at MOI 0.5. A.U., arbitrary units. **c**, LCMV Armstrong glycoprotein (GP) and nucleoprotein (NP) gene expression 4 days after intraperitoneal (i.p.) infection of wild-type (WT) and *Tfam*^{+/-} mice; *n* = 4. **d**, **e**, Nucleoid area (**d**) or ISG expression (**e**) of MEFs exposed to ddC for 96 h. **f**, ddC-exposed MEFs were infected with HSV-1-GFP or VSV-GFP at MOI 0.1 and imaged after 24 h. Error bars represent \pm s.e.m. of triplicate technical (**b**, **e**) or quadruplicate biological (**c**) replicates and are representative of two independent experiments. ***P* < 0.01; ****P* < 0.001.

Finally, we found that *Tfam*^{+/-} mice exhibit basally elevated ISG expression, which confers resistance to acute infection by lymphocytic choriomeningitis virus (LCMV) Armstrong (Extended Data Fig. 5a and Fig. 3c).

To probe a direct requirement for mtDNA stress in antiviral priming in TFAM-deficient cells, we used dideoxycytidine (ddC), a deoxyribonucleoside analogue that specifically inhibits mtDNA replication and decreases mtDNA nucleoid size^{2,20}. Treatment of wild-type MEFs with ddC resulted in reduced mtDNA copy number and decreased average nucleoid size without altering basal ISG expression (Extended Data Fig. 5b–d). In contrast, ddC drastically diminished mtDNA stress (that is, enlarged nucleoids measuring greater than 450 nm²) in *Tfam*^{+/-} and TF^D MEFs (Fig. 3d and Extended Data Fig. 5e), which was accompanied by attenuation of antiviral priming and basal ISG expression (Fig. 3e and Extended Data Fig. 5d, f). Moreover, ddC ablated the viral resistance phenotype of *Tfam*^{+/-} MEFs (Fig. 3f). We observed similar decreases in type I interferon production and a reduction in the viral resistance phenotype in ddC-treated TF^D BMDMs (Extended Data Fig. 5g, h, blue bars). These results demonstrate that mtDNA stress directly potentiates antiviral innate immunity.

The observation that ddC-treated wild-type BMDMs displayed reduced *Ifnb* and increased viral gene expression upon challenge with HSV-1, despite normal responses to cytosolic nucleic acids (Extended Data Fig. 5h, i, grey bars), indicates that virus-induced mtDNA stress may boost host antiviral responses, consistent with reports linking viral infection to mtDNA dysregulation^{21,22}. The alphaherpesvirus protein UL12.5, encoded by HSV-1 and HSV-2, localizes to mitochondria and promotes rapid mtDNA depletion in human cells, which we confirmed in MEFs (Extended Data Fig. 6a)^{22–24}. Since mtDNA depletion and nucleoid stress are often coupled, we explored nucleoid architecture and

abundance kinetically during HSV-1 infection. Notably, 3 h after challenge with HSV-1, mtDNA stress was readily apparent, with nucleoids less evenly distributed and enlarged (Fig. 4a). After 6 h, ~10% of nucleoids measured larger than 450 nm², and there was a significant decrease in total nucleoid intensity (Fig. 4b). After 12 h, we observed pronounced mtDNA depletion. The mtDNA stress observed 3 to 6 h after HSV-1 challenge closely mirrored that of TFAM-deficient cells (Fig. 4b), as did TFAM protein levels (Fig. 4c). MHV-68 and HSV-2 triggered mtDNA stress similar to HSV-1, indicating that mtDNA stress is a common cellular perturbation during herpesvirus infection (Extended Data Fig. 6b, c). However, induction of mtDNA stress and TFAM depletion were not a general consequence of viral infection, as cells infected with VSV, influenza, LCMV or vaccinia possessed normal mtDNA architecture, TFAM expression and copy number (Fig. 4a–c and Extended Data Fig. 6c, d).

Finally, we sought to determine whether HSV-1-induced mtDNA dysregulation is necessary to fully engage antiviral signalling. Transduction of MEFs and BMDMs with replication-incompetent retroviruses encoding only the mitochondria-targeted HSV-1 UL12 M185 gene product was sufficient to cause mitochondrial hyperfusion, nucleoid enlargement and mtDNA loss, indicative of mtDNA stress (Fig. 4d and Extended Data Fig. 7a)²⁴. UL12 M185 expression was also sufficient to trigger TFAM depletion and antiviral priming (that is, augmented ISG mRNA and protein expression) (Fig. 4e and Extended Data Fig. 7a). To explore the effect of HSV-1-induced mtDNA stress on innate antiviral responses, we employed a recombinant, UL12-deficient HSV-1 strain (Δ UL12 + UL98-FLAG) that is severely impaired in its ability to induce mtDNA stress but replicates similarly to a matched UL12-sufficient strain (Extended Data Fig. 7b, c)²⁵. Infection with Δ UL12 HSV-1 resulted in attenuated TBK1 phosphorylation and type I interferon

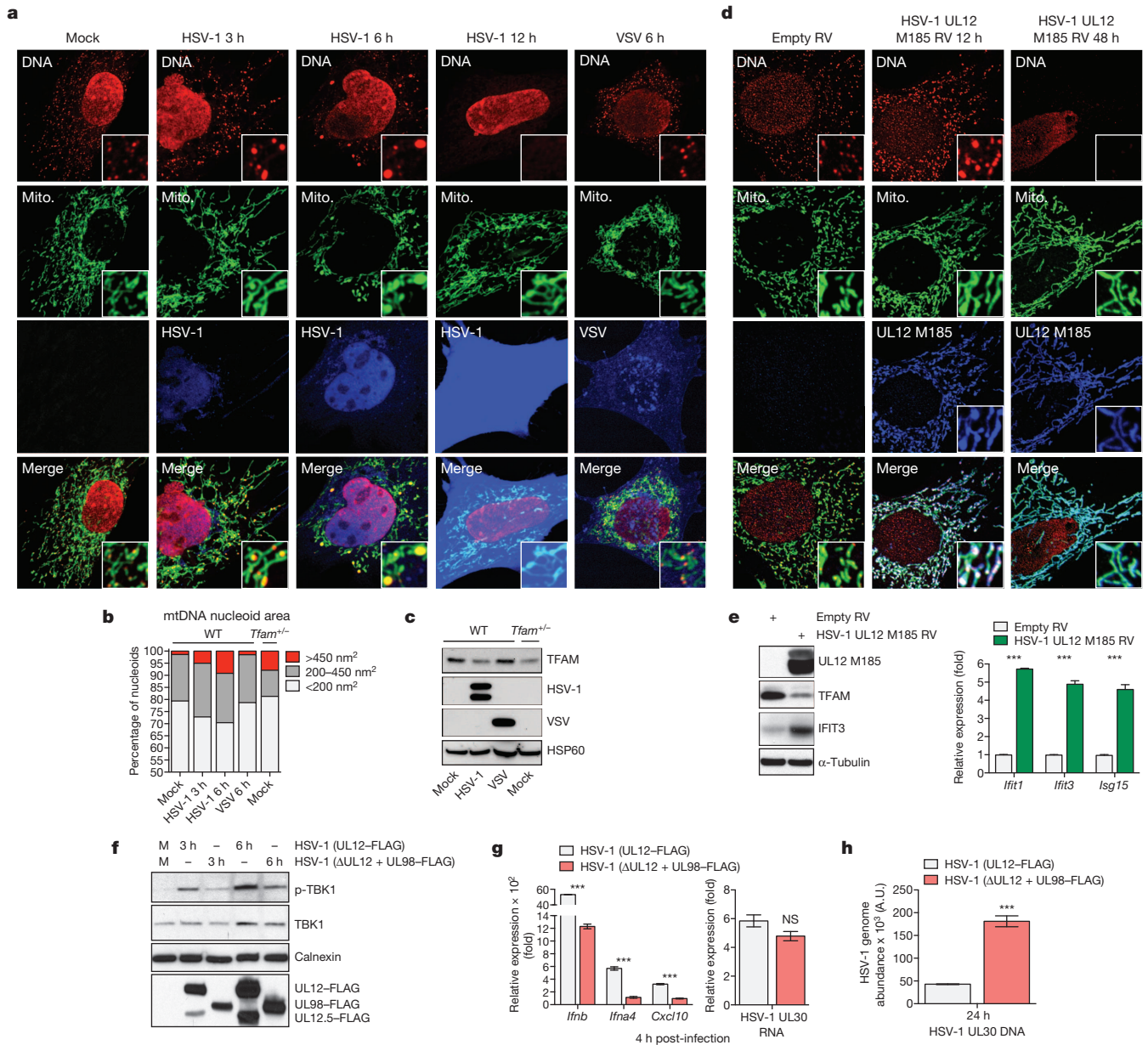


Figure 4 | HSV-1 induces mtDNA stress and TFAM depletion sufficient to trigger ISG expression and necessary to fully engage antiviral immunity. **a–c**, Wild-type (WT) MEFs were mock infected or infected with HSV-1-GFP or VSV-GFP at multiplicity of infection (MOI) 10 for the indicated times, and imaged after staining with anti-DNA (DNA), anti-HSP60 (Mito.), and anti-HSV (HSV-1) or GFP (VSV) antibodies (**a**). mtDNA nucleoid area was calculated as described in the Methods (**b**). Extracts were blotted as indicated (**c**). **d, e**, Wild-type MEFs were transduced with HSV-1 UL12 M185-FLAG-expressing or empty retroviruses (RV) and cells were stained with anti-DNA

and ISG expression between 3 to 6 h post-infection, despite comparable early HSV-1 gene expression (Fig. 4f, g). However, after 24 h, Δ UL12 HSV-1 genome abundance was roughly threefold higher compared to the UL12-sufficient control, consistent with impaired antiviral innate immunity (Fig. 4h). Finally, Δ UL12 HSV-1 elicited less robust antiviral innate immune responses in the vagina and more readily spread to dorsal root ganglia of wild-type mice due to a deficit in mtDNA stress-dependent antiviral priming (Extended Data Fig. 7d, e). These results reveal that herpesvirus-induced mtDNA stress is necessary to effectively engage ISG expression and antiviral priming, and suggest that cellular monitoring of mtDNA homeostasis represents an additional sensory mechanism to robustly engage antiviral innate immunity.

(DNA), anti-HSP60 (Mito.) and anti-FLAG antibody (UL12 M185) (**d**), and protein or ISG expression examined after 24 h (**e**). **f, g**, Protein and RNA expression in BMDMs infected with HSV-1 (UL12-FLAG) or UL12-deficient HSV-1 (Δ UL12 + UL98-FLAG) at MOI 2 for the indicated times. **h**, HSV-1 genome abundance in L929 cells that were infected as in **f, g**. A.U., arbitrary units. Error bars indicate \pm s.e.m. of triplicate technical replicates and are representative of two independent experiments. *** $P < 0.001$; NS, not significant.

In closing, our work uncovers a novel cellular response to mtDNA stress that engages the antiviral innate immune response. Specifically, we show that mtDNA stress, induced by herpesvirus infection and mediated by loss of the mtDNA packaging protein TFAM, triggers a cGAS–STING–IRF3-dependent pathway to upregulate ISGs and potentiate type I interferon responses to viral infection (Extended Data Fig. 8). Our results support a model whereby viral-mediated disruption of mtDNA homeostasis serves as a cell-intrinsic indicator of infection that works in parallel with canonical virus sensing to enhance antiviral innate immunity. Conversely, pathologic type I interferon signatures promote autoimmune diseases such as systemic lupus erythematosus, and altered ISG expression correlates with radiation-resistant and

metastatic phenotypes in some cancers^{26,27}. Mitochondrial and mtDNA dysregulation have been noted in systemic lupus erythematosus, and perturbations in TFAM and/or mtDNA homeostasis are frequently observed in cancer^{28–30}. Therefore, further investigation into this pathway will not only expand our knowledge of innate antiviral defence, but may also broaden our understanding of how mitochondria contribute to the pathogenesis of human diseases and ageing beyond their well characterized roles in metabolism, apoptosis and reactive oxygen species production.

Online Content Methods, along with any additional Extended Data display items and Source Data, are available in the online version of the paper; references unique to these sections appear only in the online paper.

Received 4 July; accepted 15 December 2014.

Published online 2 February 2015.

- Spelbrink, J. N. Functional organization of mammalian mitochondrial DNA in nucleoids: history, recent developments, and future challenges. *IUBMB Life* **62**, 19–32 (2010).
- Kasashima, K., Sumitani, M. & Endo, H. Human mitochondrial transcription factor A is required for the segregation of mitochondrial DNA in cultured cells. *Exp. Cell Res.* **317**, 210–220 (2011).
- Ryan, M. T. & Hoogenraad, N. J. Mitochondrial–nuclear communications. *Annu. Rev. Biochem.* **76**, 701–722 (2007).
- Wallace, D. C. A mitochondrial paradigm of metabolic and degenerative diseases, aging, and cancer: a dawn for evolutionary medicine. *Annu. Rev. Genet.* **39**, 359–407 (2005).
- Larsson, N. G. *et al.* Mitochondrial transcription factor A is necessary for mtDNA maintenance and embryogenesis in mice. *Nature Genet.* **18**, 231–236 (1998).
- Woo, D. K. *et al.* Mitochondrial genome instability and ROS enhance intestinal tumorigenesis in APC^{Min/+} mice. *Am. J. Pathol.* **180**, 24–31 (2012).
- Rusinova, I. *et al.* Interferome v2.0: an updated database of annotated interferon-regulated genes. *Nucleic Acids Res.* **41**, D1040–D1046 (2013).
- Schoggins, J. W. & Rice, C. M. Interferon-stimulated genes and their antiviral effector functions. *Curr. Opin. Virol.* **1**, 519–525 (2011).
- West, A. P., Shadel, G. S. & Ghosh, S. Mitochondria in innate immune responses. *Nature Rev. Immunol.* **11**, 389–402 (2011).
- Shimada, K. *et al.* Oxidized mitochondrial DNA activates the NLRP3 inflammasome during apoptosis. *Immunity* **36**, 401–414 (2012).
- Nicholls, T. J. & Minczuk, M. In D-loop: 40 years of mitochondrial 7S DNA. *Exp. Gerontol.* **56**, 175–181 (2014).
- Ban-Ishihara, R., Ishihara, T., Sasaki, N., Mihara, K. & Ishihara, N. Dynamics of nucleoid structure regulated by mitochondrial fission contributes to cristae reformation and release of cytochrome c. *Proc. Natl Acad. Sci. USA* **110**, 11863–11868 (2013).
- Malena, A., Loro, E., Di Re, M., Holt, I. J. & Vergani, L. Inhibition of mitochondrial fission favours mutant over wild-type mitochondrial DNA. *Hum. Mol. Genet.* **18**, 3407–3416 (2009).
- Cymerman, I. A., Chung, I., Beckmann, B. M., Bujnicki, J. M. & Meiss, G. EXOG, a novel paralog of Endonuclease G in higher eukaryotes. *Nucleic Acids Res.* **36**, 1369–1379 (2008).
- Sun, L., Wu, J., Du, F., Chen, X. & Chen, Z. J. Cyclic GMP-AMP synthase is a cytosolic DNA sensor that activates the type I interferon pathway. *Science* **339**, 786–791 (2013).
- Ablasser, A. *et al.* TREX1 deficiency triggers cell-autonomous immunity in a cGAS-dependent manner. *J. Immunol.* **192**, 5993–5997 (2014).
- Cai, X., Chiu, Y.-H. & Chen, Z. J. The cGAS–cGAMP–STING pathway of cytosolic DNA sensing and signaling. *Mol. Cell* **54**, 289–296 (2014).
- Atianand, M. K. & Fitzgerald, K. A. Molecular basis of DNA recognition in the immune system. *J. Immunol.* **190**, 1911–1918 (2013).
- Goubau, D., Deddouche, S. & Reis e Sousa, C. Cytosolic sensing of viruses. *Immunity* **38**, 855–869 (2013).
- Pohjoismäki, J. L. O. *et al.* Alterations to the expression level of mitochondrial transcription factor A, TFAM, modify the mode of mitochondrial DNA replication in cultured human cells. *Nucleic Acids Res.* **34**, 5815–5828 (2006).
- Wiedmer, A. *et al.* Epstein–Barr virus immediate-early protein Zta co-opts mitochondrial single-stranded DNA binding protein to promote viral and inhibit mitochondrial DNA replication. *J. Virol.* **82**, 4647–4655 (2008).
- Saffran, H. A., Pare, J. M., Corcoran, J. A., Weller, S. K. & Smiley, J. R. Herpes simplex virus eliminates host mitochondrial DNA. *EMBO Rep.* **8**, 188–193 (2007).
- Corcoran, J. A., Saffran, H. A., Duguay, B. A. & Smiley, J. R. Herpes simplex virus UL12.5 targets mitochondria through a mitochondrial localization sequence proximal to the N terminus. *J. Virol.* **83**, 2601–2610 (2009).
- Duguay, B. A. & Smiley, J. R. Mitochondrial nucleases ENDOG and EXOG participate in mitochondrial DNA depletion initiated by herpes simplex virus 1 UL12.5. *J. Virol.* **87**, 11787–11797 (2013).
- Duguay, B. A. *et al.* Elimination of mitochondrial DNA is not required for herpes simplex virus 1 replication. *J. Virol.* **88**, 2967–2976 (2014).
- Crow, M. K. & Kirou, K. A. Interferon- α in systemic lupus erythematosus. *Curr. Opin. Rheumatol.* **16**, 541–547 (2004).
- Khodarev, N. N. *et al.* Signal transducer and activator of transcription 1 regulates both cytotoxic and prosurvival functions in tumor cells. *Cancer Res.* **67**, 9214–9220 (2007).
- Lee, H.-T. *et al.* Leukocyte mitochondrial DNA alteration in systemic lupus erythematosus and its relevance to the susceptibility to lupus nephritis. *Int. J. Mol. Sci.* **13**, 8853–8868 (2012).
- Lee, H.-M., Sugino, H., Aoki, C. & Nishimoto, N. Underexpression of mitochondrial-DNA encoded ATP synthesis-related genes and DNA repair genes in systemic lupus erythematosus. *Arthritis Res. Ther.* **13**, R63 (2011).
- Wallace, D. C. Mitochondria and cancer. *Nature Rev. Cancer* **12**, 685–698 (2012).

Acknowledgements We thank N. Chandel for *Tfam*^{+/m} mice, D. Martin for *Tfam*^{+/-} MEFs, J. Schoggins and S. Virgin for *cGas*^{-/-} MEFs, G. Barber for *Sting*^{-/-} MEFs, G. Sen for IFIT3 antibodies, J. Rose for VSV antibodies and recombinant vaccinia virus, K. Bahl and J. Schell for advice with VSV infections, and S. Ding for advice with HSV-1 gene expression analysis. This work was supported by a joint grant from the United Mitochondrial Disease Foundation and Mitocin, NIH R01 AG047632 and P01 ES011163 (G.S.S.), NIH R01 AI054359 and R01 AI081884 (A.I.), Canadian Institutes for Health Research grant MOP37995 and a Canada Research Chair in Molecular Virology (J.R.S.), American Cancer Society Postdoctoral Fellowship PF-13-035-01-DMC (A.P.W.), NIH T32 AI055403 (W.K.-H.), NIH F31 AG039163 (M.C.T.), NIH NRSA F32 DK091042 (M.B.), Alberta Innovates-Health Solutions and a Queen Elizabeth II Graduate Scholarship (B.A.D.), and a United Mitochondrial Disease Foundation Postdoctoral Fellowship (N.R.).

Author Contributions A.P.W. designed and performed experiments, analysed data, interpreted results and wrote the paper; W.K.H. provided viral stocks, advice on viral infection protocols, and performed *in vivo* HSV-1 infections; M.S. performed LCMV and influenza infections; M.C.T. aided in experimental design and assisted with viral infections; C.M.P. performed experiments and analysed data; M.B. performed steady-state mitochondrial transcript analysis; N.R. assisted with gene expression array analysis; D.A.M. generated *cGas*^{-/-} MEFs; B.A.D. and J.R.S. generated and provided HSV-1 UL12 constructs and HSV-1 Δ UL12 viruses; S.M.K. provided reagents and facilities for LCMV infections and interpreted results; S.M.L. and R.E.M. provided reagents and advice and performed viral infections; A.I. supplied reagents, designed experiments, and interpreted results; G.S.S. designed experiments, interpreted results and wrote the paper.

Author Information Microarray data have been submitted to the NCBI Gene Expression Omnibus under accession number GSE63767. Reprints and permissions information is available at www.nature.com/reprints. The authors declare no competing financial interests. Readers are welcome to comment on the online version of the paper. Correspondence and requests for materials should be addressed to G.S.S. (gerald.shadel@yale.edu).

METHODS

Animal strains. *Tfam*^{+/-} and *Tfam*^{fl/fl} mice were previously described and maintained on a C57BL/6 background^{46,31}. *Tfam*^{fl/fl} mice were bred to Estrogen receptor (ER)-Cre transgenic mice from Jackson (stock no. 004682) for inducible, 4OHT-mediated deletion. All animal experiments were conducted in compliance with guidelines established by the Yale University Institutional Animal Care and Use Committee.

Antibodies and reagents. Rabbit anti-mouse TFAM polyclonal anti-sera was previously described⁶, rabbit anti-VSV polyclonal anti-sera was a gift from J. Rose at Yale University, mouse anti-Viperin was a gift from P. Cresswell at Yale University, and rabbit anti-IFIT3 was a gift from G. Sen at Cleveland Clinic. The following antibodies were obtained commercially: goat anti-HSP60 (N-20) and rabbit anti-calnexin (H-70) (Santa Cruz Biotechnology); mouse and rabbit anti-FLAG (F1804, F7425) (Sigma); mouse anti-DNA (CBL186) (Millipore); mouse anti-GFP (JL-8) (BD Biosciences); rabbit anti-HSV-1/2 (ab9533) and anti-histone H3 (ab1791) (Abcam); rat anti-HA-FITC (11988506001) (Roche); rabbit anti-NLRX1 (17215-1-AP) (Proteintech); mouse anti- α -tubulin (DM1A) (Neomarkers); mouse anti-GAPDH (6C5) (Ambion); and rabbit anti-DDX58 (D14G6), -IFIH1 (D74E4), -STAT1 (9172), -IRF3 (D83B9), -TBK1 (D1B4) and anti-phospho-TBK1 (D52C2) (Cell Signaling Technology). Mouse IFN α enzyme-linked immunosorbent assay (ELISA) and recombinant mouse IFN β was from PBL Assay Science, and mouse IL-6 ELISA was from eBioscience. All primer sequences and siRNAs used are found in Extended Data Tables 1 and 2.

Cell culture. Primary wild-type, *Tfam*^{+/-}, *Sting*^{-/-} and *cGas*^{-/-} MEFs were generated from E12.5–14.5 embryos, maintained in DMEM (Invitrogen) supplemented with 10% FBS (Atlanta Biological), and sub-cultured no more than five passages before experiments. *Sting*^{-/-} MEFs were provided by G. Barber at the University of Miami³². L929 cells were obtained from ATCC and maintained in DMEM supplemented with 10% FBS. siRNA transfection of MEFs was performed with 25 nM siRNA duplexes (Integrated DNA Technologies) and Lipofectamine RNAiMAX reagent (Invitrogen) according to the manufacturer's instructions. ddC (Sigma) was resuspended in PBS, added to MEFs or BMDMs at a final concentration of 10–20 μ M, and replenished every 48 h. BMDMs were generated from bone marrow of 8–12-week-old littermate *Tfam*^{fl/fl} ER-cre⁻ and *Tfam*^{fl/fl} ER-cre⁺ mice and cultured on Petri plates in DMEM containing 10% FBS plus 30% L929 culture media. To induce Cre-mediated deletion, 1 μ M 4OHT dissolved in DMSO (Sigma) was added to BMDM cultures on day 6 and incubated for an additional 2–3 days. Cells were then lifted from plates by incubating in cold PBS containing 1 mM EDTA, replated in fresh media containing 10% L929 conditioned media, and allowed to rest overnight before experimentation (for a total of 72 or 96 h of 4OHT exposure). Transfection of interferon-stimulatory DNA (ISD)³³ and poly(I:C) (Sigma) into the cytosol of BMDMs was performed using Lipofectamine 2000 (Invitrogen). In brief, 1 \times 10⁶ BMDMs were seeded in 6-well dishes after 4OHT treatment, and transfected the next day with 4 μ g ISD per well or 2.5 μ g per well of poly(I:C) complexed at a ratio of 2:1 Lipofectamine 2000 to nucleic acid. Poly(I:C) transfection into the cytosol of MEFs was performed as described previously³⁴.

Viral stocks and infections. VSV-G-GFP³⁵, HSV-1-GFP³⁶, MHV-68-GFP, HSV-2³⁷, vaccinia virus (strain WR) expressing bacteriophage T7 RNA polymerase³⁸, influenza A PR8 NS1-GFP³⁹, HSV-1 (UL12-FLAG) and HSV-1 (UL12 Δ + UL98-FLAG)²⁵ were maintained as described previously^{34,40,41}. MEFs or BMDMs were infected at the indicated multiplicity of infection (MOI) in serum-free DMEM for 1 h, washed, and incubated for various times. Cells were then fixed and stained for microscopy, lysed for western blot, solubilized in buffer RLT Plus (Qiagen) for RNA extraction, or prepared for FACS analysis. FACS was performed by first trypsinizing MEFs, followed by labelling with LIVE/DEAD Fixable Far Red stain (Molecular Probes). Cells were then fixed with 4% paraformaldehyde, washed, and analysed on a FACSCalibur flow cytometry machine (BD). FACS plots were first gated on live cells before analysing viral GFP fluorescence. Viral gene expression in BMDMs was determined using qRT-PCR as described below, except that after values were normalized against GAPDH cDNA using the 2^{- $\Delta\Delta$ C_T} method, all data points were subtracted by one to centre on zero.

LCMV Armstrong infection of wild-type and *Tfam*^{+/-} mice was performed as described previously⁴². In brief, 10-week-old female mice were infected with 2 \times 10⁷ plaque-forming units of virus intraperitoneally, and 4 days post-infection, mice were euthanized, tissues isolated, and total RNA prepared using RNeasy Plus kits (QIAGEN). After generating complementary DNA, samples were subjected to qPCR analysis as described below using published methods^{43,44}.

In vivo HSV-1 infection, dorsal root ganglia isolation and viral titration. Six-week-old female mice were purchased from Charles River Laboratories and treated with Depo Provera (GE Healthcare) 5 days before infection⁴⁵. The vaginal canals of Depo Provera treated mice were swabbed with a Calginate swab (Fisher) and 10⁶ plaque-forming units were delivered via pipette tip into the vagina. One day post-infection, vaginal tissue was isolated for RNA extraction. Infected mice were

euthanized at indicated time points and dorsal root ganglia were dissected as previously described⁴⁶. Dorsal root ganglia were homogenized using a motorized pestle and total DNA was isolated using the DNeasy Blood & Tissue Kit (Qiagen) according to the manufacturer's instructions. Relative HSV-1 genome abundance was determined using primers specific for nuclear *Tert* and HSV-1 *TK* (thymidine kinase).

cGAS-HA and UL12 M185 cloning and retroviral expression. A plasmid encoding HSV-1 UL12 M185 SPA containing a 3 \times FLAG tag at the carboxy-terminus was described previously²⁴. This construct, or a plasmid encoding murine cGAS-HA (Invivogen), was sub-cloned into the pMXs-IRES-Puro vector and replication incompetent retroviruses were packaged using plat-E cells according to the manufacturer's instructions (Cell Biolabs). SV40 large T immortalized cGAS^{-/-} MEFs were exposed to supernatants containing cGAS-HA retroviruses and incubated overnight. Two days post-transduction, 3 μ g ml⁻¹ puromycin was added to select a stable population of cells expressing cGAS-HA. Supernatants containing empty or UL12 M185 SPA retroviruses and 4 μ g ml⁻¹ polybrene were incubated with cells (5 \times 10⁴ MEFs or 2 \times 10⁵ BMDMs) in 12-well dishes for a period of 8 h. Viral supernatants were then washed off, fresh media was added to wells, and the cells were incubated for the duration of the experiment until lysis.

Quantitative PCR. To measure relative gene expression by qRT-PCR, total cellular RNA was isolated using RNeasy Plus RNA extraction kit (Qiagen). Approximately 400–2000 ng RNA was normalized across samples and cDNA was generated using the High Capacity cDNA RT kit (Applied Biosystems). cDNA was then subjected to qPCR using Fast SYBR Green Master Mix (Applied Biosystems) and primers as indicated on the ViiA7 Real Time PCR system (Life Technologies). Three technical replicates were performed for each biological sample, and expression values of each replicate were normalized against GAPDH cDNA using the 2^{- $\Delta\Delta$ C_T} method. For relative expression (fold), control samples were centred at 1; for relative expression (%), control samples were centred at 100%. Mitochondrial DNA copy number analysis was performed as described using primers specific to nuclear *Tert* and the D-loop region of mtDNA (listed in Extended Data Table 1)⁶. Relative HSV-1 genome abundance was determined using primers specific for nuclear *Tert* and HSV-1 *UL30* or *TK*. Relative MHV68 genome abundance was determined using primers specific for nuclear *Tert* and MHV68 *orf40*. Relative vaccinia genome abundance was determined using primers specific for nuclear *Tert* and vaccinia virus DNA polymerase *E9L*.

Immunofluorescence microscopy. For all microscopy images containing mtDNA nucleoids and associated panels, cells were grown on coverslips and transfected, treated, and/or infected as described. After washing in PBS, cells were fixed with 4% paraformaldehyde for 20 min, permeabilized with 0.1% Triton X-100 in PBS for 5 min, blocked with PBS containing 10% FBS for 30 min, stained with primary antibodies for 60 min, and stained with secondary antibodies for 60 min. Cells were washed with PBS between each step. Coverslips were mounted with Prolong Gold anti-fade reagent containing DAPI (4',6-diamidino-2-phenylindole; Molecular Probes). Cells were imaged on a Zeiss LSM 510 META with a 63 \times water-immersed objective. A digital scan zoom of 3.0 was used to enhance magnification. Images were pseudo-coloured and merged using ImageJ software (NIH). For microscopy images in Fig. 3, MEFs were infected as described and fixed with 4% paraformaldehyde for 20 min. Viral GFP fluorescence and phase contrast images were captured using an Olympus IX-71 inverted scope with a 10 \times (Fig. 3a) or 20 \times (Fig. 3f) objective. Viral GFP images were pseudo-coloured using ImageJ.

For nucleoid area quantification, approximately 10–15 unique fields of view from 10 distinct confocal images, comprising between 200–400 nucleoids, were captured at random. After incorporating scale information obtained from the LSM Image Browser (Zeiss), images were made binary and the area of each nucleoid was determined using the 'Analyze Particles' feature of ImageJ. Nucleoids were divided into the three size cut-offs: <200 nm²; 200–450 nm²; and >450 nm², and the percentage of nucleoids falling within each category was plotted. The percentage of nucleoids >450 nm² displaying cGAS co-localization was scored by calculating nucleoid area from 5 distinct images of siCtrl- and si*Tfam*-transfected cGAS-HA reconstituted MEFs as described above. Nucleoids larger than 450 nm² with a substantial cGAS co-localization signal were scored as positive.

Electron microscopy. MEFs grown in Petri dishes and on coverslips for orientation were fixed in 2.5% glutaraldehyde in 0.1 M sodium cacodylate buffer pH 7.4 for 1 h. The cells were rinsed in sodium cacodylate and those in Petri dishes were scraped and spun down in 2% agar. All samples were fixed in 1% osmium tetroxide for 1 h, stained en masse in 2% uranyl acetate in maleate buffer pH 5.2 for a further hour, rinsed and dehydrated in an ethanol series, and infiltrated with resin (Embed812 EMS) and baked overnight at 60 °C. Hardened blocks were cut using a Leica UltraCut UCT. 60-nm sections were collected on formvar/carbon-coated grids and contrast stained using 2% uranyl acetate and lead citrate. Samples were viewed on an FEI Tencai Biotwin TEM at 80 Kv. Images were taken using Morada CCD and iTEM (Olympus) software.

For mitochondrial perimeter quantification, approximately 10–15 unique electron microscopy images of each genotype were captured at random. After incorporating scale information from iTEM software, the perimeter along the outer membrane of each mitochondrion was traced and quantified using ImageJ. Mitochondria were divided into the three size cutoffs: <2 μm ; 2–5 μm ; and >5 μm , and the percentage of mitochondria falling within each category was plotted.

Oxygen consumption analysis. Cells were plated in XF96 plates (SeaHorse Biosciences) at 10,000 cells per well and the next day cellular O_2 consumption was determined in a SeaHorse Bioscience XF96 extracellular flux analyser according to the manufacturer's instructions. Cells were maintained at 37 °C in normal growth medium without serum.

Nuclear fractionation and western blotting. Whole-cell extracts were solubilized in SDS lysis buffer (20 mM Tris-HCl, 1% SDS, pH 7.5, containing protease and phosphatase inhibitors), boiled for 5 min, and DNA was sheared by sonication. For nuclear extraction, PBS-washed cell pellets were resuspended in 10 pellet volumes of RSB buffer (10 mM NaCl, 1.5 mM CaCl_2 , 10 mM Tris-HCl pH 7.5), swelled on ice for 10 min, homogenized with a motorized Teflon pestle, and the homogenate was centrifuged at 980g for 10 min to pellet nuclei. Pellets were washed five times in PBS, SDS was then added to a final concentration of 1%, and extracts were boiled for 5 min before sonicating to shear DNA and normalizing protein concentration. Western blotting was performed using standard protocols, and HSP60 was used as whole-cell extract loading controls, while histone H3 was probed as a nuclear loading control.

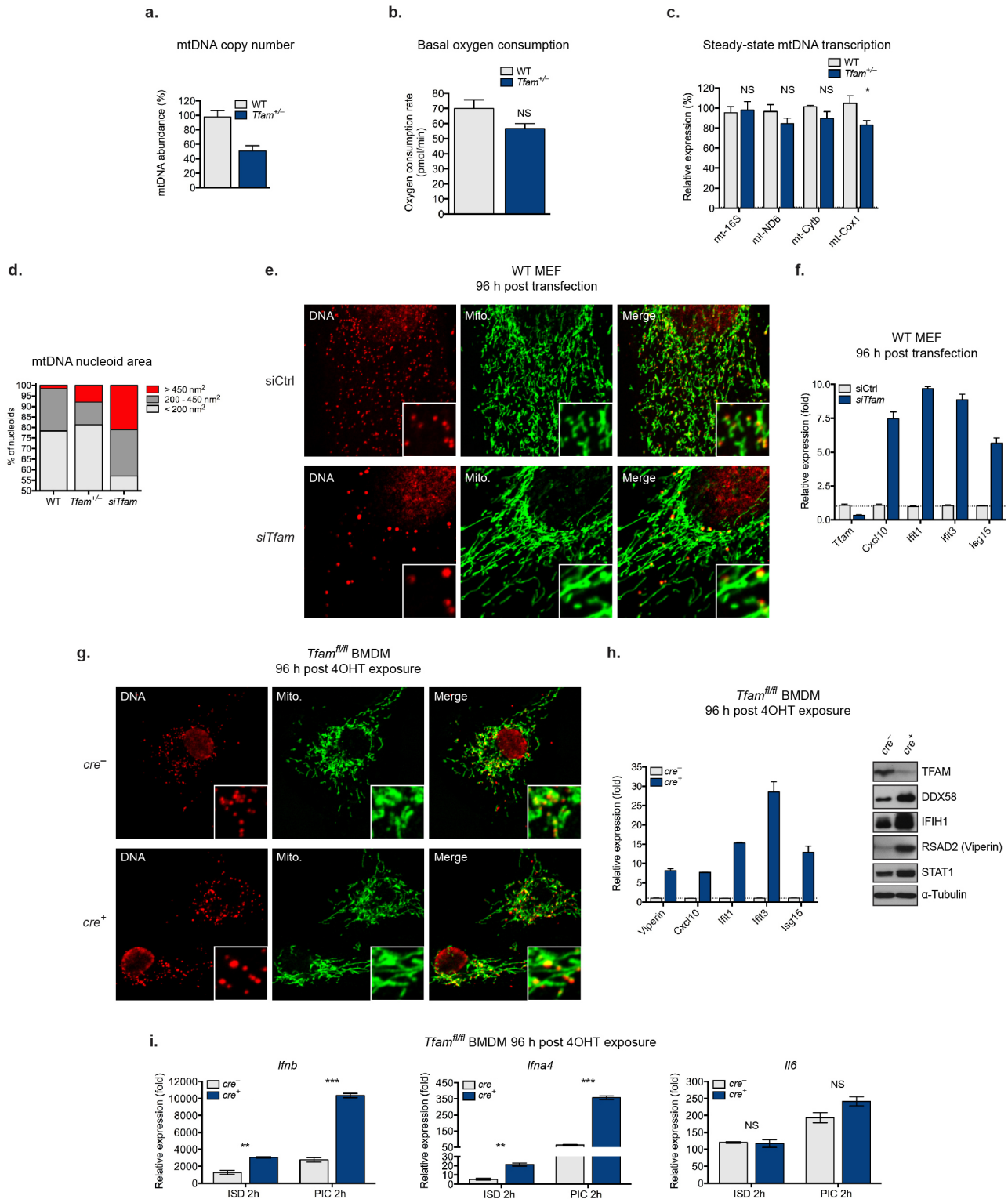
Detection of mtDNA in cytosolic extracts. Digitonin extracts from MEFs and BMDMs were generated largely as described previously⁴⁷. Wild-type and *Tfam*^{+/-} MEFs (7×10^6) or *Tfam*^{fl/fl} *ER-cre*^{+/-} BMDMs exposed to 4OHT for 72 h (1×10^7) were each divided into two equal aliquots, and one aliquot was resuspended in 500 μl of 50 μM NaOH and boiled for 30 min to solubilize DNA. 50 μl of 1 M Tris-HCl pH 8 was added to neutralize the pH, and these extracts served as normalization controls for total mtDNA. The second equal aliquots were resuspended in roughly 500 μl buffer containing 150 mM NaCl, 50 mM HEPES pH 7.4, and 15–25 $\mu\text{g ml}^{-1}$ digitonin (EMD Chemicals). The homogenates were incubated end over end for 10 min to allow selective plasma membrane permeabilization, then centrifuged at 980g for 3 min three times to pellet intact cells. The first pellet was saved as the 'Pel' fraction for western blotting. The cytosolic supernatants were transferred to fresh tubes and spun at 17000g for 10 min to pellet any remaining cellular debris, yielding cytosolic preparations free of nuclear, mitochondrial and endoplasmic reticulum contamination. DNA was then isolated from these pure cytosolic fractions using QIAquick Nucleotide Removal Columns (QIAGEN). Quantitative PCR was performed on both whole-cell extracts and cytosolic fractions using nuclear DNA primers (*Tert*) and mtDNA primers (*Dloop1-3*, *Cytb*, *16S* and *Nd4*), and the C_T values obtained for mtDNA abundance for whole-cell extracts served as normalization controls for the mtDNA values obtained from the cytosolic fractions. This allowed effective standardization among samples and controlled for any variations in the total amount of mtDNA in control and TFAM-deficient samples. Using this digitonin method, no nuclear *Tert* DNA was detected in the cytosolic fractions, indicating nuclear lysis did not occur.

Bioinformatic analyses. Total cellular RNA from wild-type and *Tfam*^{+/-} littermate MEFs was prepared using RNeasy Plus RNA extraction kits (QIAGEN) and used for the expression microarray procedure in conjunction with the Emory University Integrated Genomics Core. RNA integrity was first verified by an Agilent Bioanalyzer and then amplified, labelled, and hybridized onto Mouse Gene 1.0 ST arrays (Affymetrix) using standard protocols recommended by the manufacturer, starting from 2 μg of total RNA. Data were normalized by the RMA method using

GeneSpring software (Agilent) for each biological sample in duplicate. Student's *t*-test was used to determine statistically significant changes in expression in *Tfam*^{+/-} MEFs relative to wild type, with a cut-off *P* value of 0.05⁴⁸. Heat maps were generated using MultiExperiment Viewer⁴⁹.

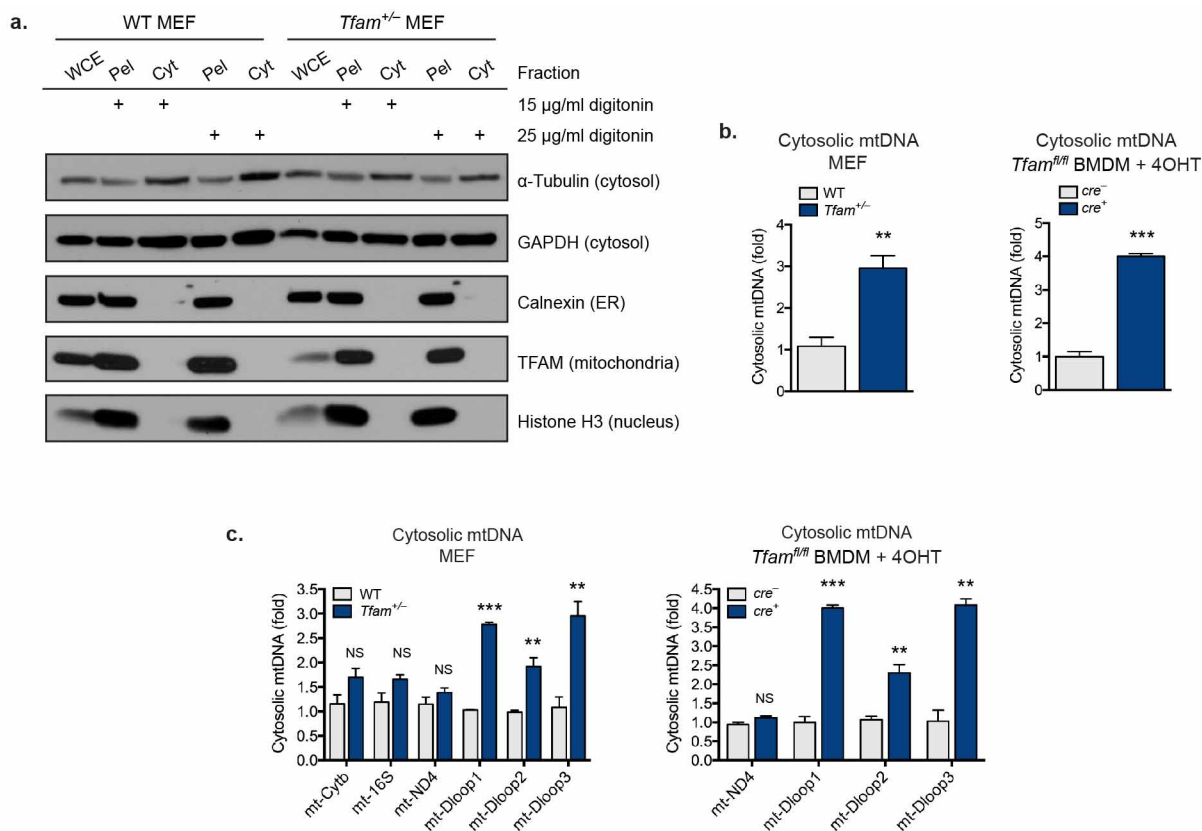
Statistical analyses. Error bars displayed throughout the manuscript represent s.e.m. unless otherwise indicated, and were calculated from triplicate or quadruplicate technical replicates of each biological sample. For *in vivo* experiments, error bars were calculated from the average of triplicate technical replicates of 3–4 mice per point. Sample sizes were chosen by standard methods to ensure adequate power, and no randomization or blinding was used for animal studies. No statistical method was used to predetermine sample size. Statistical significance was determined using unpaired Student's *t*-tests; **P* < 0.05; ***P* < 0.01; ****P* < 0.001; NS, not significant (*P* > 0.05). Data shown are representative of 2–3 independent experiments, including microscopy images, western blots and viral challenges.

- Weinberg, F. *et al.* Mitochondrial metabolism and ROS generation are essential for Kras-mediated tumorigenicity. *Proc. Natl Acad. Sci. USA* **107**, 8788–8793 (2010).
- Ishikawa, H. & Barber, G. N. STING is an endoplasmic reticulum adaptor that facilitates innate immune signalling. *Nature* **455**, 674–678 (2008).
- Stetson, D. B. & Medzhitov, R. Recognition of cytosolic DNA activates an IRF3-dependent innate immune response. *Immunity* **24**, 93–103 (2006).
- Tal, M. C. *et al.* Absence of autophagy results in reactive oxygen species-dependent amplification of RLR signaling. *Proc. Natl Acad. Sci. USA* **106**, 2770–2775 (2009).
- Dalton, K. P. & Rose, J. K. Vesicular stomatitis virus glycoprotein containing the entire green fluorescent protein on its cytoplasmic domain is incorporated efficiently into virus particles. *Virology* **279**, 414–421 (2001).
- Desai, P. & Person, S. Incorporation of the green fluorescent protein into the herpes simplex virus type 1 capsid. *J. Virol.* **72**, 7563–7568 (1998).
- Shin, H. & Iwasaki, A. A vaccine strategy that protects against genital herpes by establishing local memory T cells. *Nature* **491**, 463–467 (2012).
- Fuerst, T. R., Niles, E. G., Studier, F. W. & Moss, B. Eukaryotic transient-expression system based on recombinant vaccinia virus that synthesizes bacteriophage T7 RNA polymerase. *Proc. Natl Acad. Sci. USA* **83**, 8122–8126 (1986).
- Pang, I. K., Pillai, P. S. & Iwasaki, A. Efficient influenza A virus replication in the respiratory tract requires signals from TLR7 and RIG-I. *Proc. Natl Acad. Sci. USA* **110**, 13910–13915 (2013).
- Yordy, B., Iijima, N., Huttner, A., Leib, D. & Iwasaki, A. A neuron-specific role for autophagy in antiviral defense against herpes simplex virus. *Cell Host Microbe* **12**, 334–345 (2012).
- Cardenas, I. *et al.* Placental viral infection sensitizes to endotoxin-induced pre-term labor: a double hit hypothesis. *Am. J. Reprod. Immunol.* **65**, 110–117 (2011).
- Marshall, H. D. *et al.* Differential expression of Ly6C and T-bet distinguish effector and memory Th1 CD4⁺ cell properties during viral infection. *Immunity* **35**, 633–646 (2011).
- Welsh, R. M. & Seedhom, M. O. Lymphocytic choriomeningitis virus (LCMV): propagation, quantitation, and storage. *Curr. Protoc. Microbiol.* **Unit 15A. 1**, <http://dx.doi.org/10.1002/9780471729259.mc15a01s8> (2008).
- McCausland, M. M. & Crotty, S. Quantitative PCR technique for detecting lymphocytic choriomeningitis virus *in vivo*. *J. Virol. Methods* **147**, 167–176 (2008).
- Parr, M. B. *et al.* A mouse model for studies of mucosal immunity to vaginal infection by herpes simplex virus type 2. *Lab. Invest.* **70**, 369–380 (1994).
- Malin, S. A., Davis, B. M. & Molliver, D. C. Production of dissociated sensory neuron cultures and considerations for their use in studying neuronal function and plasticity. *Nature Protocols* **2**, 152–160 (2007).
- Holden, P. & Horton, W. A. Crude subcellular fractionation of cultured mammalian cell lines. *BMC Res. Notes* **2**, 243 (2009).
- Raimundo, N. *et al.* Mitochondrial stress engages E2F1 apoptotic signaling to cause deafness. *Cell* **148**, 716–726 (2012).
- Saeed, A. I. *et al.* TM4: a free, open-source system for microarray data management and analysis. *Biotechniques* **34**, 374–378 (2003).



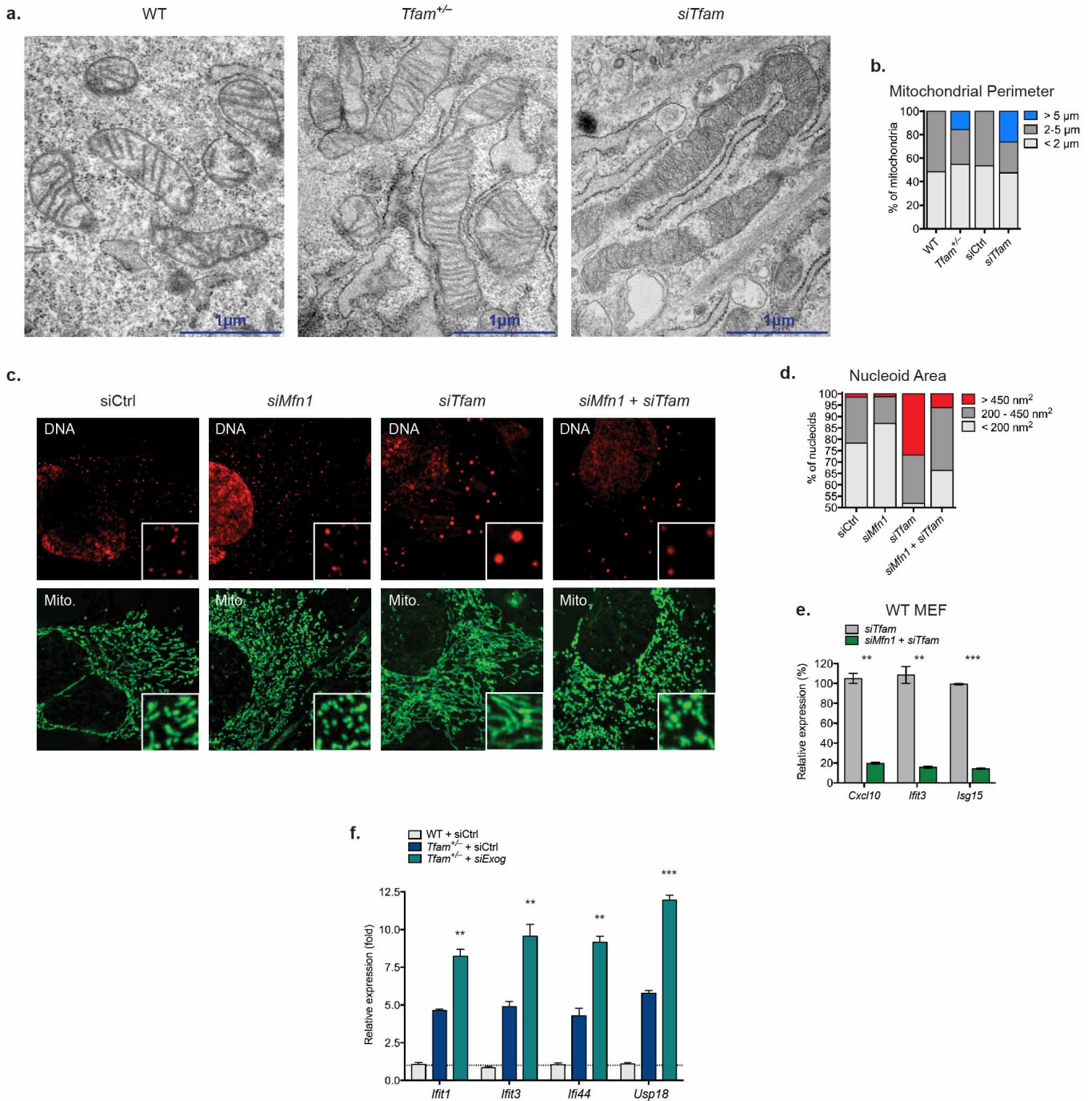
Extended Data Figure 1 | TFAM deficiency induces mtDNA depletion, nucleoid stress, elevated ISG expression and augmented type I interferon responses, but does not drastically alter oxygen consumption and mitochondrial transcription rates. **a**, Quantitative PCR analysis of relative mtDNA copy number from wild-type (WT) and *Tfam*^{+/-} MEFs. **b**, Basal oxygen consumption rate of wild-type and *Tfam*^{+/-} MEFs as determined by Seahorse Bioscience XF96 Extracellular Flux assay. **c**, qRT-PCR of mtDNA-encoded rRNA (16s) and mRNA (ND6, Cytb, Cox1) transcripts in wild-type and *Tfam*^{+/-} MEFs. **d-f**, Untransfected *Tfam*^{+/-} (**d**) or wild-type MEFs transfected with control (siCtrl) or *Tfam* (*siTfam*) siRNAs (**d-f**) were stained with anti-HSP60 (Mito.) and anti-DNA (DNA) antibodies. Nucleoid area from multiple independent images was calculated, stratified into groups, and

graphed as percentage of the total number of nucleoids counted for each sample (**d**). Inset panels are 3 \times magnification to enhance viewing of mitochondrial network and nucleoid architecture (**e**). TFAM and ISG mRNA expression were measured by qRT-PCR (**f**). **g-i**, *Tfam*^{fl/fl} *ER-cre*⁻ or *Tfam*^{fl/fl} *ER-cre*⁺ BMDMs were incubated in 4OHT for 96 h to induce TFAM depletion. Immunofluorescence staining was performed as described above (**g**). ISG mRNA and protein expression was monitored by qRT-PCR and western blotting (**h**). qRT-PCR analysis of type I interferon and *Il6* expression in 4OHT-treated *Tfam*^{fl/fl} *ER-cre*^{-/+} BMDMs 2 h post-cytosolic delivery of interferon-stimulatory DNA (ISD) or poly(I:C) (**i**). Error bars indicate \pm s.e.m. of triplicates and data are representative of three independent experiments. **P* < 0.05; ***P* < 0.01; ****P* < 0.001; NS, not significant.



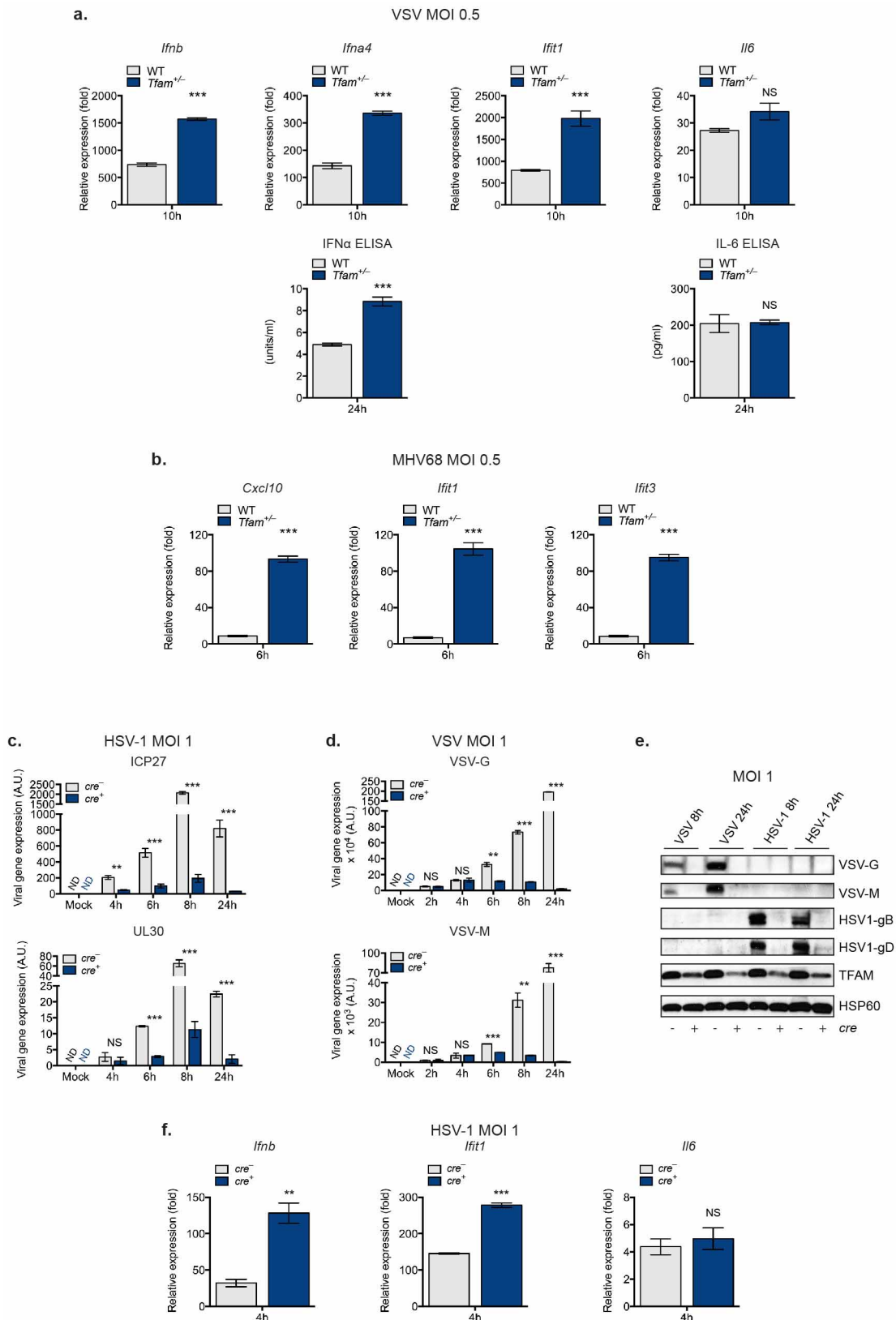
Extended Data Figure 2 | TFAM deficiency promotes accumulation of cytosolic mtDNA. **a.** Wild-type (WT) or *Tfam*^{+/-} MEFs were subjected to digitonin fractionation as described in the Methods and whole-cell extracts (WCE), pellets (Pel) or cytosolic extracts (Cyt) were blotted using the indicated antibodies. **b.** DNA was extracted from digitonin extracts of wild-type and *Tfam*^{+/-} MEFs or *Tfam*^{fl/fl} ER-cre⁻ or *Tfam*^{fl/fl} ER-cre⁺ BMDMs incubated in

4OHT for 72 h. Cytosolic mtDNA was quantitated via qPCR using a mitochondrial *Dloop* primer set (mt-Dloop3). Normalization was performed as described in the Methods. **c.** Samples were prepared as described in **b.**, and cytosolic mtDNA was quantitated via qPCR using the indicated primer sets. Error bars indicate \pm s.e.m. of triplicates and data are representative of three independent experiments. ** $P < 0.01$, *** $P < 0.001$.



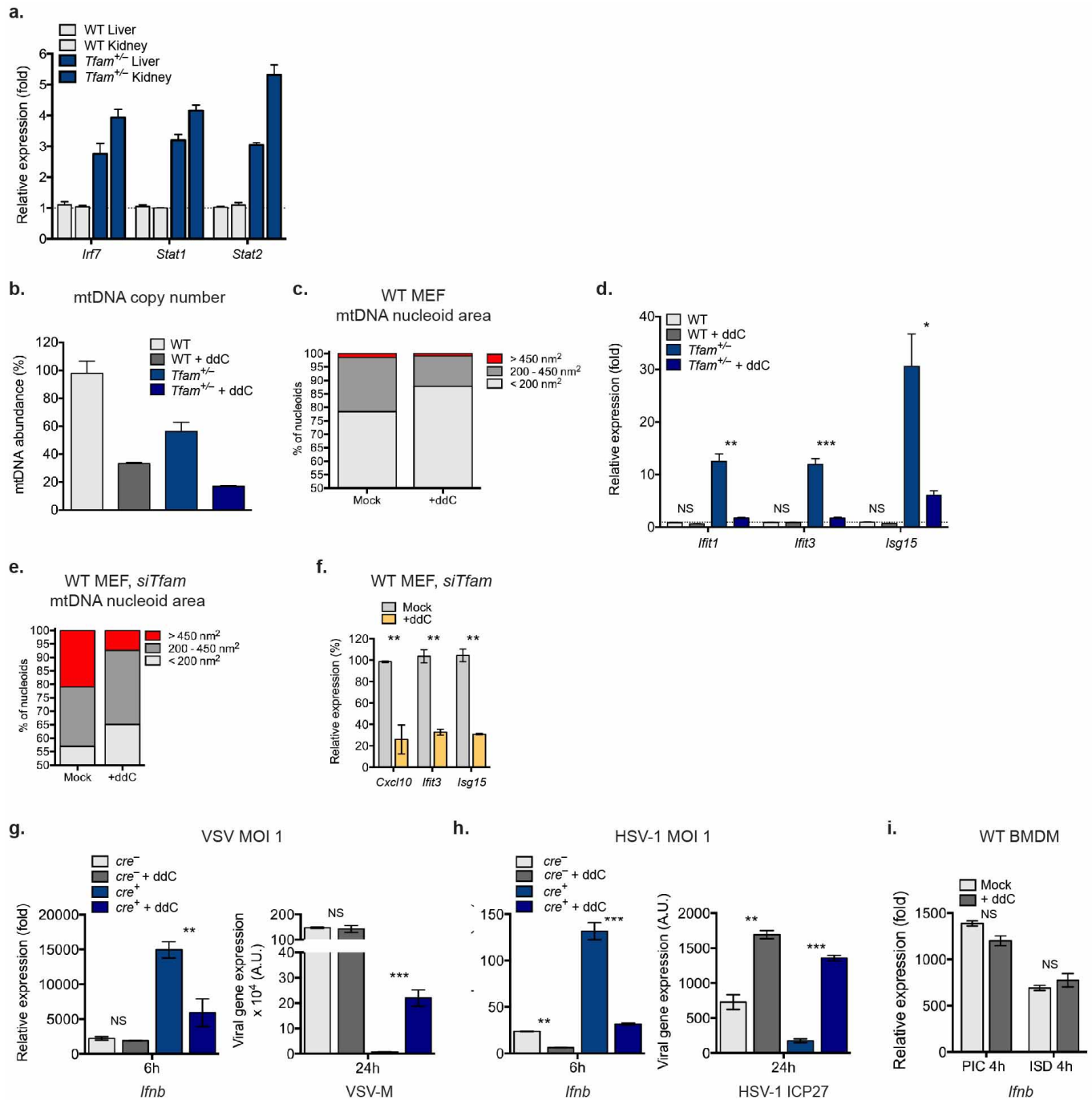
Extended Data Figure 3 | Mitochondrial hyperfusion regulates the accumulation of mtDNA nucleoid stress in TF^D MEFs. **a, b,** Wild-type (WT) MEFs were transfected with control or *Tfam* siRNAs for 96 h. Cells were fixed and processed for electron microscopy analysis (**a**). Mitochondrial perimeter measurements were obtained from multiple independent images, stratified into groups, and graphed as a percentage of the total number of mitochondria counted for each sample (**b**). **c–e,** Wild-type MEFs were transfected with control, *Mfn1* and/or *Tfam* siRNAs for 96 h. Cells were fixed and stained with

an anti-HSP60 antibody (Mito.) and an anti-DNA antibody (DNA) for confocal microscopy (**c**). Nucleoid area from multiple independent images was calculated as previously described (**d**). RNA was extracted for ISG expression analysis by qRT-PCR (**e**). **f,** Wild-type and *Tfam*^{+/-} MEFs were transfected with the indicated siRNAs for 96 h and ISG expression analysed by qRT-PCR. Error bars indicate ± s.e.m. of triplicates and data are representative of two independent experiments. ***P* < 0.01; ****P* < 0.001.



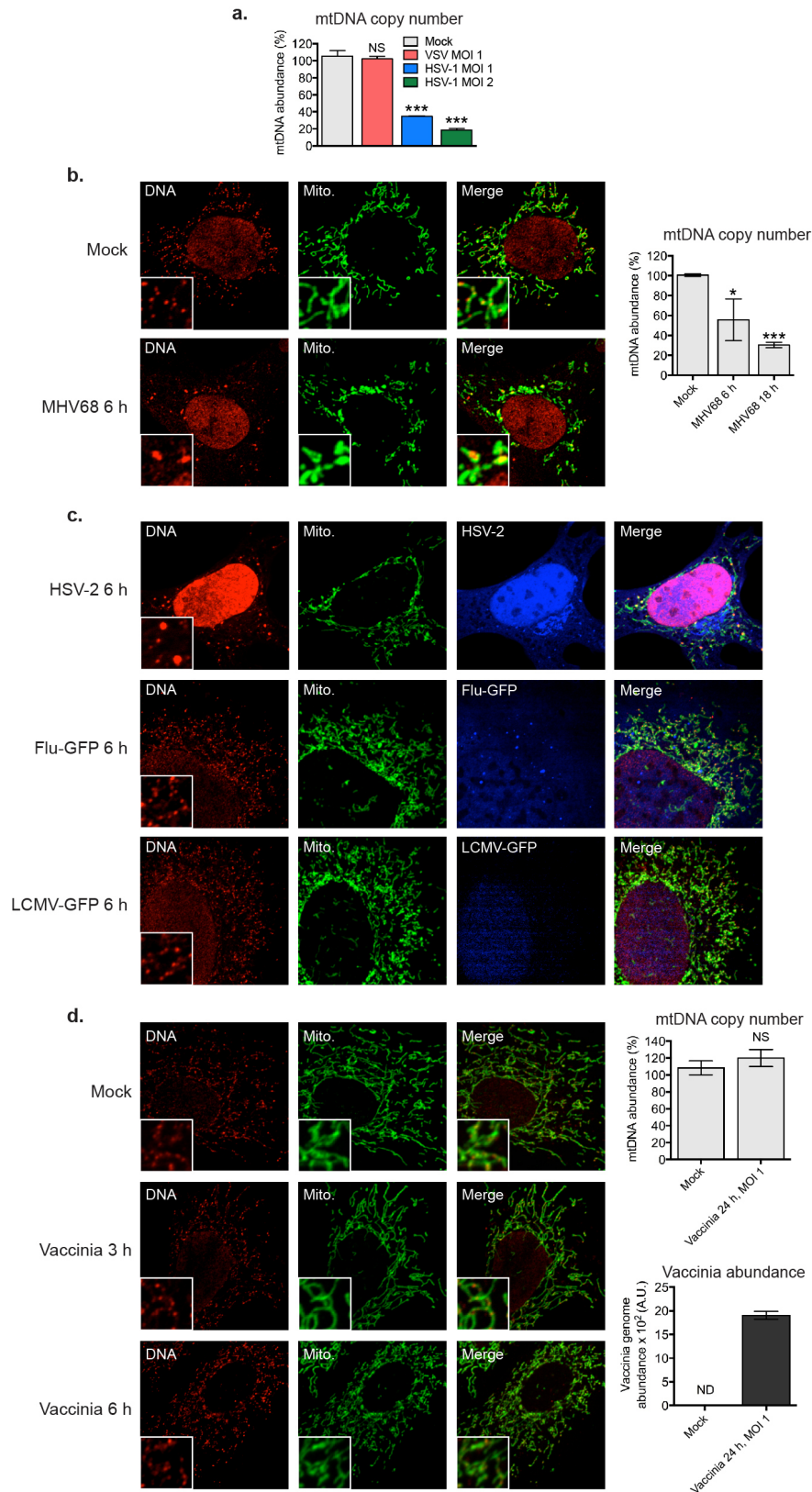
Extended Data Figure 4 | mtDNA stress in TF^D MEFs and BMDMs potentiates type I interferon responses to viral infection and enhances viral clearance. **a, b,** Wild-type (WT) and $Tfam^{+/-}$ MEFs were infected with VSV-GFP (**a**) or MHV68-GFP (**b**) and, after the indicated times, cytokine and ISG mRNA expression was determined by qRT-PCR, or cytokine secretion was determined by ELISA. **c–f,** $Tfam^{fl/fl} ER-cre^{-}$ or $Tfam^{fl/fl} ER-cre^{+}$ BMDMs were incubated in 4OHT for 96 h to induce TFAM depletion. Cells were infected

with HSV-1-GFP (**c, e, f**) or VSV-GFP (**d, e**), incubated for the indicated times, and viral gene expression was determined by qRT-PCR (**c, d**) and western blotting (**e**), or cytokine and ISG mRNA expression was determined by qRT-PCR (**f**). Error bars indicate \pm s.e.m. of triplicates and data are representative of two independent experiments. ** $P < 0.01$; *** $P < 0.001$; A.U., arbitrary units; ND, not detected; NS, not significant.



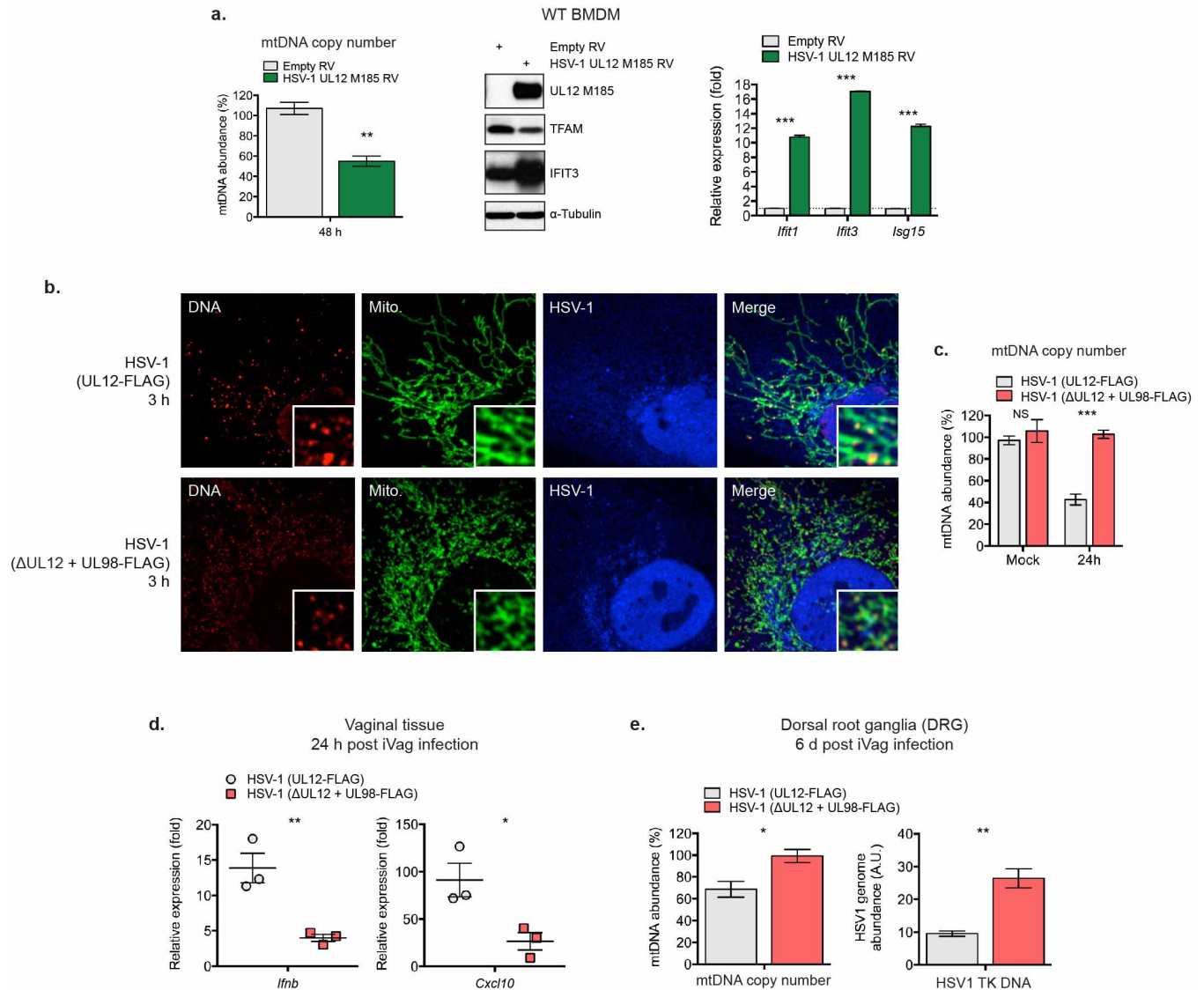
Extended Data Figure 5 | Tissues from *Tfam*^{+/-} mice display elevated ISG expression, and ddC abrogates mtDNA stress, ISG expression and viral resistance phenotypes of TF^D cells. **a**, RNA was extracted from the liver and kidneys of 8-week-old wild-type (WT) and *Tfam*^{+/-} mice ($n = 2$ each) and subjected to qRT-PCR analysis for basal ISG expression. **b-d**, Relative mtDNA copy number (**b**), mtDNA nucleoid area (**c**) and ISG expression (**d**) of wild-type and *Tfam*^{+/-} MEFs exposed to ddC for 96 h. **e, f**, mtDNA nucleoid area (**e**) and ISG expression (**f**) of wild-type MEFs transfected with control or *Tfam* siRNAs for 96 h in the presence or absence of ddC. **g-i**, *Tfam*^{fl/fl} *ER-cre*⁻ or

Tfam^{fl/fl} *ER-cre*⁺ BMDMs were incubated in 4OHT for 96 h to induce TFAM depletion in the presence of ddC. ddC was washed out and cells allowed to recover overnight before infection. Cells were infected with VSV-GFP (**g**) or HSV-1-GFP (**h**) at MOI 1, or wild-type BMDMs were transfected with poly(I:C) or interferon-stimulatory DNA (ISD) (**i**), and incubated for the indicated times. *Ifnb* expression or viral gene expression was determined by qRT-PCR. Error bars indicate \pm s.e.m. of triplicates and data are representative of two independent experiments. * $P < 0.05$; ** $P < 0.01$; *** $P < 0.001$; NS, not significant.



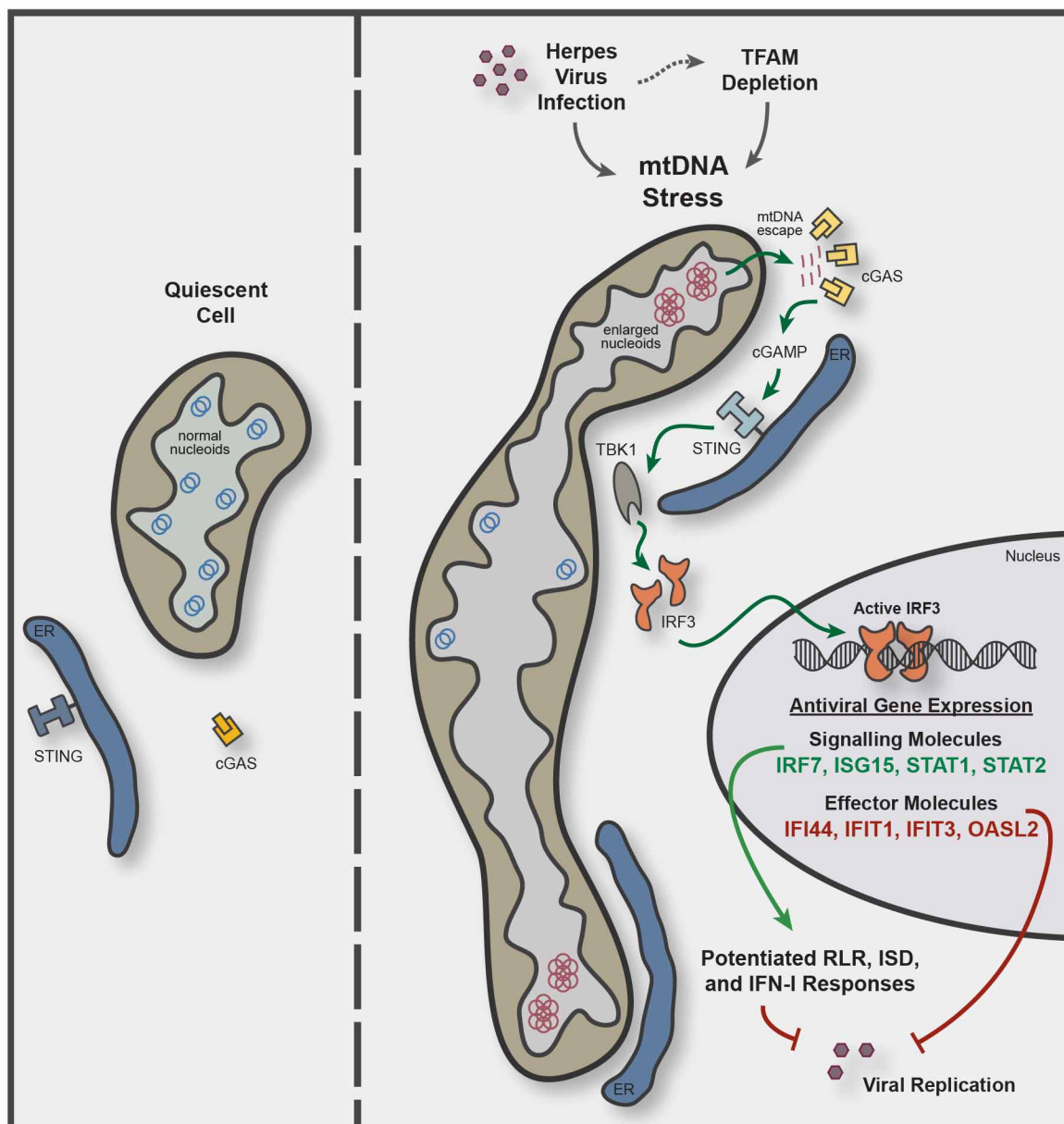
Extended Data Figure 6 | Alpha- and gammaherpesviruses induce mtDNA stress, but influenza, LCMV, and vaccinia do not. **a**, Relative mtDNA copy number of wild-type (WT) MEFs 24 h post-infection with VSV-GFP, HSV-1-GFP or mock infection at the indicated MOIs. **b**, Wild-type MEFs were infected with MHV68-GFP at MOI 0.5. After the indicated times cells were stained and subjected to confocal microscopy or the relative mtDNA copy number was determined. **c**, Wild-type MEFs were infected with HSV-2,

influenza-GFP or LCMV-GFP at MOI 10. After 6 h, cells were stained and subjected to confocal microscopy. **d**, Wild-type MEFs were infected with vaccinia virus at MOI 10 (for microscopy) or 1. After the indicated times cells were stained and subjected to confocal microscopy or the relative mtDNA copy number was determined. Error bars indicate \pm s.e.m. of triplicates and data are representative of two independent experiments. * $P < 0.05$; ** $P < 0.01$; *** $P < 0.001$; A.U., arbitrary units; ND, not detected; NS, not significant.



Extended Data Figure 7 | HSV-1 UL12 M185 expression is sufficient to trigger mtDNA stress, TFAM depletion and antiviral priming in BMDMs; infection with UL12-deficient HSV-1 fails to induce mtDNA stress, elicits lower vaginal type I interferon responses and spreads more readily to dorsal root ganglia. **a**, Wild-type (WT) BMDMs were transduced with HSV-1-UL12-M185-expressing- or empty retroviruses (RV) and relative mtDNA abundance, protein expression, and ISG mRNA expression determined. **b**, Wild-type MEFs were infected with HSV-1 (UL12-FLAG) or UL12-deficient HSV-1 (Δ UL12 + UL98-FLAG) at MOI 10 for 3 h and analysed by confocal microscopy. **c**, Wild-type MEFs were infected with HSV-1 (UL12-FLAG) or UL12-deficient HSV-1 (Δ UL12 + UL98-FLAG) at MOI 2 for 24 h and

mtDNA abundance was determined by qPCR. **d**, The vaginas of wild-type mice ($n = 3$ per condition) were inoculated with 10^6 plaque-forming units of HSV-1 (UL12-FLAG) or UL12-deficient HSV-1 (Δ UL12 + UL98-FLAG) and 24 h post-infection, vaginal RNA was extracted and gene expression analysed by qRT-PCR. **e**, Mice ($n = 3$ per condition) were infected as previously described and 6 days post-infection, DNA from dorsal root ganglia was isolated for mtDNA and HSV-1 genome abundance measurements by qPCR. Error bars indicate \pm s.e.m. of triplicates and data are representative of two independent experiments. * $P < 0.05$; ** $P < 0.01$; *** $P < 0.001$; NS, not significant.



Extended Data Figure 8 | Model illustrating mtDNA stress-dependent antiviral priming. TFAM depletion, induced genetically or during herpesvirus infection, triggers mtDNA stress, characterized by nucleoid loss and enlargement. This results in the release of fragmented mtDNA that recruits and activates peri-mitochondrial cGAS to generate the second messenger cyclic GMP-AMP (cGAMP) and activate endoplasmic-reticulum-resident STING. STING then activates TBK1, which phosphorylates IRF3 to induce dimerization and nuclear translocation. Active IRF3 elevates basal gene

expression of ISGs with antiviral signalling and effector functions. Signalling molecules encoded by ISGs, such as IRF7, ISG15, STAT1 and STAT2, cooperate with IRF3 to potentiate the RIG-I-like receptor (RLR), interferon-stimulatory DNA (ISD) and type I interferon (IFN-I) responses, while effector molecules encoded by ISGs, such as IFI44, IFIT1, IFIT3 and OASL2, augment viral resistance. Both outcomes collectively and robustly boost innate antiviral defences to dampen viral replication.

Extended Data Table 1 | Oligonucleotides used in qPCR

| Gene name | Forward and reverse oligo. sequences |
|------------------|--|
| mGapdh | GACTTCAACAGCAACTCCCAC TCCACCACCCTGTTGCTGTA |
| mTfam | AAGGATGATTCGGCTCAGG GGCTTTGAGACCTAACTGG |
| mmt-16S | GTTACCCTAGGATAACAGCGC GATCCAACATCGAGGTCGTAAACC |
| mmt-ND6 | TTAGCATTAAAGCCTTCACC CCAACAAACCCACTAACAAT |
| mmt-Cytb | AGTAGACAAAGCCACCTTGA CCGCGATAATAAATGGTAAG |
| mmt-Cox1 | GCCCCAGATATAGCATTCCC GTTTCATCCTGTTCTGCTCC |
| mlfna4 | CTTTCTCATGATCCTGGTAAATGAT AATCCAAAATCCTTCTGTCTCTC |
| mlfnb | CCCTATGGAGATGACGGAGA CCCAGTGCTGGAGAAATTGT |
| mlI6 | TGATGCACTTGACAGAAAACA ACCAGAGGAAATTTTCAATAGGC |
| mViperin | ATAGTGAGCAATGGCAGCCT AACCTGCTCATCGAAGCTGT |
| mlfit1 | CAAGGCAGGTTTCTGAGGAG GACCTGGTCACCATCAGCAT |
| mlfit3 | TTCCCAGCAGCACAGAAAC AAATTCCAGGTGAAATGGCA |
| mlfi44 | CTGATTACAAAAGAAGACATGACAGAC AGGCCAAAACCAAGACTCCA |
| mlsg15 | CTAGAGCTAGAGCCTGCAG AGTTAGTCACGGACACCAG |
| mUsp18 | GAGAGGACCATGAAGAGGA TAAACCAACCAGACCATGAG |
| mlrf7 | CAATTCAGGGGATCCAGTTG AGCATTGCTGAGGCTCACTT |
| mCycl10 | CCAAGTGCTGCCGTCATTTTC GGCTCGCAGGGATGATTTC |
| mStat1 | CGCGCATGCAACTGGCATATAACT ATGCTTCGGTCCCACGTAGACTT |
| mStat2 | TGATCTCTAACAGACAGGTGG CTGCATTCACTTCTAAGGACTC |
| mMda5 | CGGAAGTTGGAGTCAAAGC TTTGTTCACTCTGAGTCATGG |
| mRig-I | GAGTACCACTTAAAGCCAGAG AATCCATTTCTTCAAGCATCC |
| HSV1 ICP27 RNA | TTTCTCCAGTGCTACCTGAAGG TCAACTCGCAGACACGACTCG |
| HSV1 UL30 RNA | CGCGCTTGGCGGGTATTAACAT TGGGTGTCCGGCAGAATAAAGC |
| VSV G | CAAGTCAAAATGCCCAAGAGTCACA TTTCTTGCATTGTTCTACAGATGG |
| VSV M | TATGATCCGAATCAATTAAGATATG GGGACGTTTCCCTGCCATTCCGATG |
| LCMV GP | TGCCTGACCAATGGATGATT CTGCTGTGTTCCCGAAACT |
| LCMV NP | CAGAAATGTTGATGCTGGACTGC CAGACCTGGCTTGCTTACACAG |
| MHV68 gDNA ORF40 | TAGCCACACCTCCCACGC ATTCAGACCTGAACATAGTGC |
| Vaccinia E9L | CGGCTAAGAGTTGCACATCCA CTCTGCTCCATTTAGTACCGATTCT |
| HSV1 gDNA TK | ATACCGACGATCTGCGACCT TTATTGCCGTCATAGCGCGG |
| HSV1 gDNA UL30 | ATCACCGACCCGAGAG CAGGCGCTTGTGGTGT |
| m.mtDNA Dloop 1 | AATCTACCATCCTCCGTGAAACC TCAGTTTAGCTACCCCAAGTTTAA |
| m.mtDNA Dloop 2 | CCCTCCCCATTTGGTCT TGGTTTACGGAGGATGG |
| m.mtDNA Dloop 3 | TCCTCCGTGAAACCAACAA AGCGAGAAGAGGGGCATT |
| m.mtDNA CytB | GCTTTCCACTTCATCTTACCATTTA TGTTGGGTTGTTTATCCTG |
| m.mtDNA 16S | CACTGCCTGCCAGTGA ATACCGCGCCGTTAAA |
| m.mtDNA ND4 | AACGGATCCACAGCCGTA AGTCTCGGGCCATGATT |
| m.nucDNA Tert | CTAGCTCATGTGTCAAGACCCTCTT GCCAGCACGTTTCTCTCGTT |

Extended Data Table 2 | Dicer substrate siRNAs used

| Gene name | IDT Duplex name |
|------------------------------|------------------------|
| mTfam | MMC.RNAI.N009360.12.1 |
| mExoG | MMC.RNAI.N172456.12.1 |
| mSting | MMC.RNAI.N028261.12.1 |
| mcGas | MMC.RNAI.N173386.12.1 |
| mTbk1 | MMC.RNAI.N019786.12.1 |
| mIrf3 | MMC.RNAI.N016849.12.1 |
| mMfn1 | MMC.RNAI.N024200.12.1 |
| Firefly luciferase (si-Ctrl) | FLuc-S1 |

All siRNAs were predesigned by Integrated DNA Technologies and transfected at 25 nM final concentration.